

# Superior Performance of Microporous Aluminophosphate with LTA Topology in Solar-Energy Storage and Heat Reallocation

Andraž Krajnc, Jure Varlec, Matjaž Mazaj, Alenka Ristić, Nataša Zabukovec Logar,\* and Gregor Mali\*

Hydrophilic porous materials are recognized as very promising materials for water-sorption-based energy storage and transformation. In this study, a porous, zeolite-like aluminophosphate with LTA (Linde Type A) topology is inspected as an energy-storage material. The study is motivated by the material's high predicted pore volume. According to sorption and calorimetric tests, the aluminophosphate outperforms all other zeolite-like and metal-organic porous materials tested so far. It adsorbs water in an extremely narrow relative-pressure interval ( $0.10 < p/p_0 < 0.15$ ) and exhibits superior water uptake ( $0.42 \text{ g g}^{-1}$ ) and energy-storage capacity ( $527 \text{ kW h m}^{-3}$ ). It also shows remarkable cycling stability; after 40 cycles of adsorption/desorption its capacity drops by less than 2%. Desorption temperature for this material, which is one of crucial parameters in applications, is lower from desorption temperatures of other tested materials by 10–15 °C. Furthermore, its heat-pump performance is very high, allowing efficient cooling in demanding conditions (with cooling power up to  $350 \text{ kW h m}^{-3}$  even at 30 °C temperature difference between evaporator and environment). On the microscopic scale, sorption mechanism in  $\text{AlPO}_4\text{-LTA}$  is elucidated by X-ray diffraction, nuclear magnetic resonance measurements, and first-principles calculations. In this aluminophosphate, energy is stored predominately in hydrogen-bonded network of water molecules within the pores.

that porous materials could be very useful in the exploitation of solar energy and waste heat in adsorption-driven heat-transformation applications, because they could offer very efficient energy storage.<sup>[1–7]</sup> Energy from renewable sources could be used to dry a porous material, which could then be stored in the obtained “excited/charged” state without thermal losses. At a later stage, when water was returned into the porous material in a controllable way, upon the adsorption of water molecules into the pores the stored energy would be released as sensible heat.

A good sorption-based energy-storage material should fulfill the following requirements: (i) it should exhibit high water uptake at low relative humidity, (ii) it should be easily regenerated at low temperature, and (iii) it should be highly hydrothermally stable and should enable good cycling (adsorption/desorption) performance. So far, several types of porous materials have been considered for energy storage, but most of them failed to meet at least one of the above criteria. For example, porous amorphous silica gels

offered too low water uptake, whereas aluminosilicate zeolites typically required too high regeneration temperatures. Versatile porous metal-organic framework materials (MOFs) have also been studied. Recently, Furukawa et al. and Cadiau et al. have presented stable, hydrophilic metal-organic framework materials MOF-801 and MIL-160 with high water uptakes of 0.36 and 0.38 g per 1 g of the dried matrix, respectively.<sup>[8,9]</sup> These materials adsorbed large fractions of water in a relatively narrow range of pressures ( $p/p_0$  range of 0.05–0.20), and could be quite efficiently regenerated at temperatures below 100 °C.

Several investigations showed that zeolite-like microporous aluminophosphates might also act as effective sorption-based energy-storage materials.<sup>[2,10–13]</sup> Ristić et al. described the performance of the most promising aluminophosphate so far,  $\text{AlPO}_4\text{-34}$ .<sup>[12]</sup> In the temperature range between 40 °C and 140 °C this material exhibited similar storage capacity as MOF-801 and MIL-160, it was hydrothermally very stable and enabled reversible adsorption and desorption without a significant decrease of the storage capacity. Most importantly,  $\text{AlPO}_4\text{-34}$

## 1. Introduction

In our efforts to reduce air pollution and global warming, more and more attention is devoted to research and development of technologies for the effective exploitation of renewable energy resources. Over the last decade, several studies have proposed

A. Krajnc, J. Varlec, Dr. M. Mazaj, Dr. A. Ristić,  
Prof. N. Z. Logar, Prof. G. Mali  
National Institute of Chemistry  
Hajdrihova 19, SI-1001 Ljubljana, Slovenia  
E-mail: natasa.zabukovec@ki.si; gregor.mali@ki.si  
A. Krajnc  
Jozef Stefan International Postgraduate School  
Jamova cesta 39, SI-1000 Ljubljana, Slovenia  
Prof. N. Z. Logar  
University of Nova Gorica  
Vipavska 13, SI-5000 Nova Gorica, Slovenia



DOI: 10.1002/aenm.201601815

adsorbed water much more suddenly, i.e., in a much narrower relative-pressure interval, and could be more efficiently regenerated at low temperatures than MIL-160 and MOF-801. The reason for the sudden water uptake in  $\text{AlPO}_4\text{-34}$  is in the quick formation of energetically very favorable ordered hydrogen-bonded water clusters within the pores.<sup>[14]</sup> It is proposed that the formation of these clusters is facilitated by the tendency of the framework aluminum atoms to attract water molecules and to rapidly and reversibly change coordination environment from tetrahedral to octahedral.

In the search for an even better energy-storage material with even higher capacity and equally sudden water uptake as  $\text{AlPO}_4\text{-34}$ , we focused on  $\text{AlPO}_4\text{-LTA}$ , a microporous aluminophosphate analogous to LTA-type aluminosilicate (Linde Type A), which is built of double-four-rings (D4R), sodalite, and LTA cages (also called beta and alpha cages, respectively). The accessible pore volume of  $\text{AlPO}_4\text{-LTA}$  is expected to be somewhat larger than the volume of  $\text{AlPO}_4\text{-34}$  with chabazite topology; according to the database of zeolite structure types the accessible pore volumes for the LTA and chabazite topologies are 21% and 17%, and their densities are 14.2 and 15.1 tetrahedral (aluminum and phosphorus) atoms per 1000  $\text{\AA}^3$ , respectively.<sup>[15,16]</sup>

$\text{AlPO}_4\text{-LTA}$  can be synthesized along several different routes, using up to three different structure directing agents (SDAs). Irrespective of the synthesis route, the calcination of the synthesized products, i.e., the removal of the SDA species from the pores, seems to be problematic, as all the researchers reported partial loss of crystallinity and/or collapse of the microporous structure of  $\text{AlPO}_4\text{-LTA}$  upon thermal treatment.<sup>[17–19]</sup> Perhaps the best results so far were described by Huang et al., who prepared  $\text{AlPO}_4\text{-LTA}$  membrane from fluoride medium with Kryptofix 222 (K222) as SDA and calcined the material in the mixture of air and ozone, using very slow heating with maximal temperature of 300 °C, and by Fayad et al., who prepared  $\text{AlPO}_4\text{-LTA}$  powder with ionothermal synthesis in fluoride medium using 1-benzyl-3-methylimidazolium (BenzMIM) ionic liquid and tetramethylamine (TMA).<sup>[20,21]</sup> In this latter case, the authors claim that heating the as-synthesized material to 400 °C expelled BenzMIM<sup>+</sup> cations from the larger LTA cages, but could not remove TMA<sup>+</sup> cations from the smaller sodalite cages.

For the sorption-based energy-storage application it is crucial that the storage material has empty pores and that it is hydrothermally stable. That is why, in the first step of this work, we focused on calcination. In the next step, we thoroughly inspected the successfully calcined material as an energy-storage material and proved that its water uptake and energy-storage capacity significantly exceed the ones of  $\text{AlPO}_4\text{-34}$ , MOF-801, and MIL-160, which were until now considered as the most promising water-sorption-based energy-storage materials. Finally, we tried to explain why microporous aluminophosphates are at the moment probably the best known materials for water-sorption-based energy storage.

## 2. Results and Discussion

We prepared  $\text{AlPO}_4\text{-LTA}$  in fluoride medium with hydrothermal synthesis using K222 as the structure directing agent.<sup>[17]</sup> X-ray diffraction (XRD) confirmed that the prepared aluminophosphate

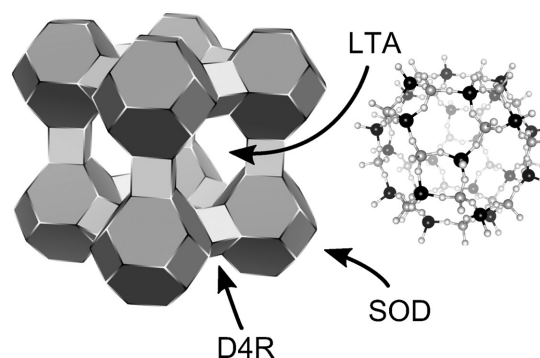


**Figure 1.** Schematic representation of the aluminophosphate framework of  $\text{AlPO}_4\text{-LTA}$ . The framework comprises double-four-rings (D4R), sodalite (SOD), and LTA cages. In the scheme on the left, the vertices show the positions of the tetrahedrally coordinated Al and P atoms, and the solid lines represent the Al–O–P bridges. In the scheme on the right, the details of the LTA cage are presented (black spheres, Al; grey spheres, P; small white spheres, O). LTA cage is one of the largest cages encountered in the family of porous aluminophosphates.

was highly crystalline and exhibited the LTA topology (Figure S1, Supporting Information). **Figure 1** schematically shows that the basic building units of  $\text{AlPO}_4\text{-LTA}$  are D4Rs, which are connected one to another in such a way that larger sodalite cages are formed. Eight sodalite cages arranged in the corners of a cube encircle the even larger LTA cage. In  $\text{AlPO}_4\text{-LTA}$ , the vertices of the LTA cage are 24 aluminum and 24 phosphorus atoms. The inner diameters of the sodalite and LTA cages are  $\approx 6.3$  and 11.0  $\text{\AA}$ , respectively, and the diameters of the largest windows to these cages are 2.5  $\text{\AA}$  (six-membered ring) for the sodalite cage and 4.2  $\text{\AA}$  (eight-membered ring) for the LTA cage.

### 2.1. Calcination of $\text{AlPO}_4\text{-LTA}$

The crucial step toward successful calcination of  $\text{AlPO}_4\text{-LTA}$  was to follow thermal treatment of the as-synthesized materials in situ by XRD. The measurements show that the material prepared with K222 is stable and very well crystalline up to about 900 °C in air (see **Figure 2**). Even at this highest temperature the diffraction peaks are not broadened, only their intensities change. The peaks also slightly shift with temperature, indicating that  $\text{AlPO}_4\text{-LTA}$  with empty pores shows small, nearly linear negative thermal expansion (Figure S2, Supporting Information). The material that is obtained with calcination in air at 850 °C is a white powder without an NMR-detectable content of carbon. <sup>31</sup>P and <sup>27</sup>Al magic-angle spinning (MAS) NMR spectra each exhibit a strong sharp peak corresponding to tetrahedrally coordinated phosphorus and aluminum atoms, respectively. They also show very weak, broad contributions that can be assigned to an amorphous aluminophosphate impurity representing less than 5% of the sample (Figure S3, Supporting Information). Even though  $\text{AlPO}_4\text{-LTA}$  is a microporous aluminophosphate with one of the largest possible cages, the presented results show that it is remarkably thermally stable and can thus be calcined easily.

The calcined material is very hygroscopic. As shown in **Figure 2**, adsorption of water into  $\text{AlPO}_4\text{-LTA}$  substantially

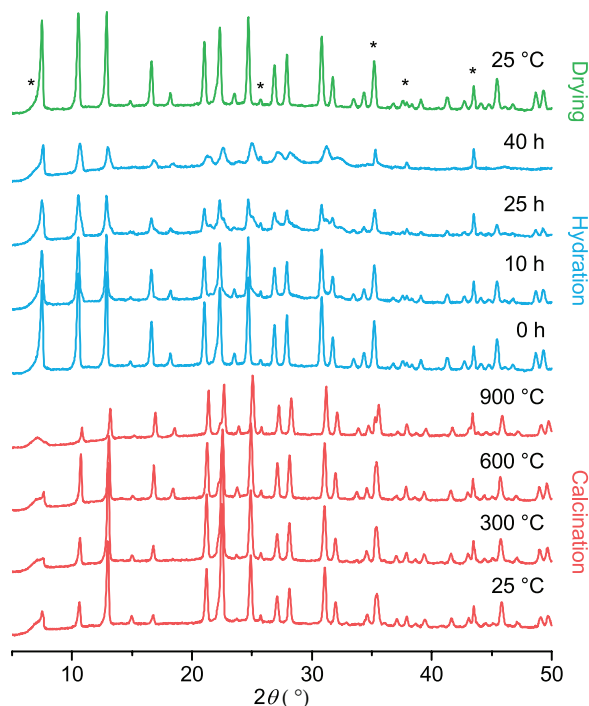


**Figure 2.** XRD patterns of  $\text{AlPO}_4\text{-LTA}$  recorded during in situ calcination (red), hydration at 25 °C and relative humidity of 30% (blue), and after drying at 100 °C for 1 h (green). Asterisks indicate the positions of diffraction peaks of  $\text{Al}_2\text{O}_3$  sample holder and Kapton foil. The last step shows that although hydration broadens the diffraction peaks, it does not destroy the aluminophosphate framework and the material can be reversibly dehydrated.

broadens the peaks in the diffraction pattern. In earlier investigations, researchers probably observed such broadening and misinterpreted it as being due to the partial degradation of the aluminophosphate framework upon calcination. As we shall see later, the framework is not damaged by hydration and in fact the dehydration/rehydration process is completely reversible.

## 2.2. $\text{AlPO}_4\text{-LTA}$ as an Energy-Storage Material

For the evaluation of the energy-storage potential of  $\text{AlPO}_4\text{-LTA}$ , we used the material that was calcined in air at 850 °C. The material exhibits an extremely steep water-sorption isotherm and a remarkable water uptake of  $0.36 \text{ g g}^{-1}$  in the relative-pressure range between 0.05 and 0.20 (**Figure 3**). Such an uptake is the largest known among microporous aluminophosphates, substantially larger than the uptake of  $\text{AlPO}_4\text{-34}$ , and it greatly exceeds the uptakes of MIL-160 and MOF-801 in a comparably narrow pressure range. Hydration/dehydration of  $\text{AlPO}_4\text{-LTA}$  is completely reversible and the cycling test shows that the capacity for water sorption drops by less than 2% after 40 cycles.  $^{27}\text{Al}$  and  $^{31}\text{P}$  MAS NMR spectra indicate that the loss of capacity is due to a small increase of the fraction of the disordered aluminophosphate phase in the sample, which can be detected as a weak broad signal with  $^{31}\text{P}$  chemical shifts between  $-10$  and  $-30$  ppm and a weak signal with  $^{27}\text{Al}$  shifts between 30 and 0 ppm. This suggests that the repeated hydration

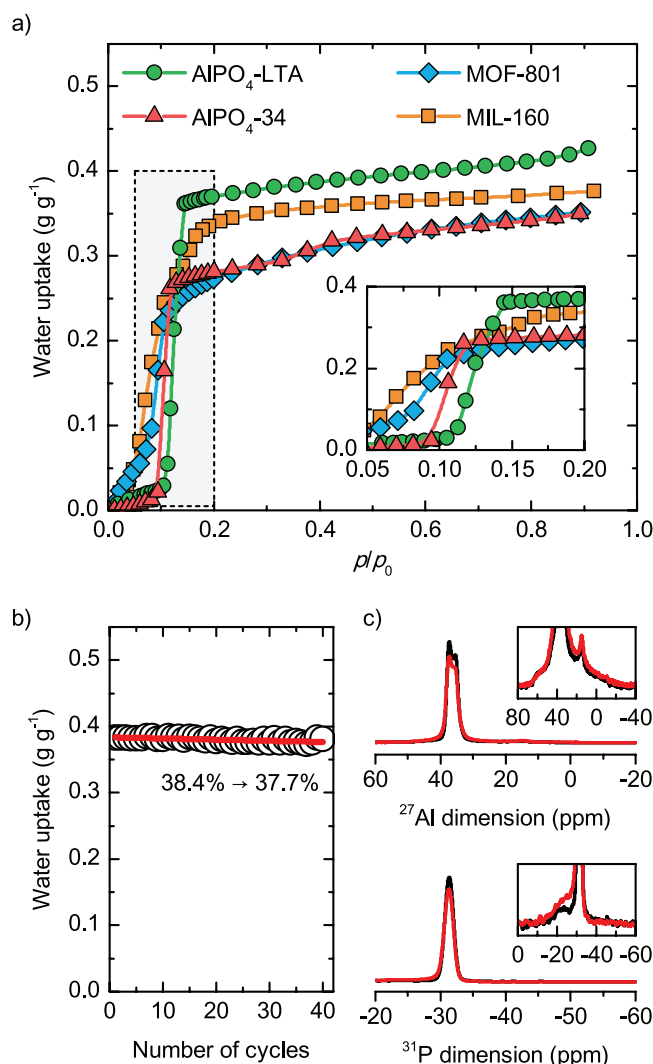


**Figure 3.** a) Water sorption isotherms for  $\text{AlPO}_4\text{-LTA}$  (green ●), MIL-160 (orange ■), MOF-801 (blue ◆), and  $\text{AlPO}_4\text{-34}$  (red ▲), recorded at 30 °C. Data for MIL-160 were obtained from the work of Cadiau et al.<sup>[9]</sup> The inset shows the marked area. b) Hydration/dehydration cycling performance of  $\text{AlPO}_4\text{-LTA}$  (hydration at 25 °C and relative pressure of 0.30, drying at 150 °C under vacuum). c)  $^{27}\text{Al}$  and  $^{31}\text{P}$  MAS NMR spectra of  $\text{AlPO}_4\text{-LTA}$ . The spectra were recorded on the fresh dehydrated sample (black) and on the same sample after 40 cycles of hydration/dehydration (red).  $\text{AlPO}_4\text{-LTA}$ , exhibiting an extremely steep adsorption isotherm and high water uptake, is remarkably stable.

and dehydration induces only hardly observable degradation of the porous aluminophosphate framework of  $\text{AlPO}_4\text{-LTA}$ .

The energy capacity of  $\text{AlPO}_4\text{-LTA}$  was evaluated by calorimetric measurements. **Figure 4** and **Table 1** compare the differential scanning calorimetry (DSC) profiles and the values of the energies that were needed to dry the samples of  $\text{AlPO}_4\text{-LTA}$ ,  $\text{AlPO}_4\text{-34}$ , and MOF-801. Details of the preparation of the latter two samples are given in the Experimental Section. As one can see,  $\text{AlPO}_4\text{-LTA}$  has the largest capacity among all, closely followed by MOF-801 and  $\text{AlPO}_4\text{-34}$ . Here two remarks are needed. First, Table 1 compares energies stored per unit volume of the materials, which, in our opinion, are more

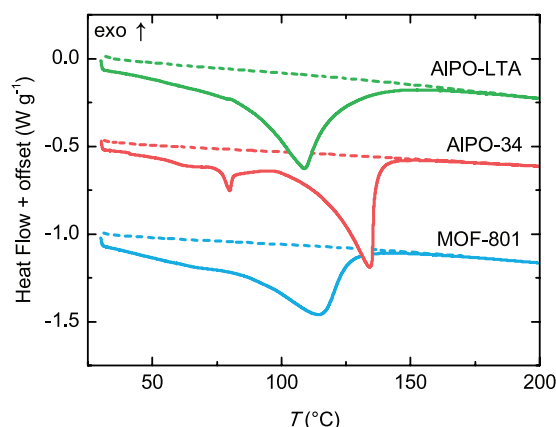


**Figure 4.** Calorimetric measurements obtained on a set of hydrated (solid lines) and dried samples (dotted lines) of AlPO<sub>4</sub>-LTA (green), AlPO<sub>4</sub>-34 (red), and MOF-801 (blue). The measurements were obtained with a temperature ramp of 1 °C min<sup>-1</sup>.

relevant for stationary applications of porous materials than the energies stored per unit of mass. The latter might be important for mobile applications, in which not only the volume of the storage unit but also its mass matters. Second, whereas for certain zeolites even larger energy-storage capacities than the one of AlPO<sub>4</sub>-LTA were calculated, the required temperatures for the complete regeneration of these materials are well above 200 °C. In contrast, both aluminophosphates and MOF-801 can be regenerated at very low temperature and reasonably low humidity. For example, with a flow of dry air at 25 °C, AlPO<sub>4</sub>-LTA, AlPO<sub>4</sub>-34, and MOF-801 can be completely dehydrated whereas a representative of the aluminosilicate zeolites, zeolite 4A, remains almost fully hydrated (Figure S4, Supporting Information).

In the above-described DSC experiment, energy that is needed to dry a given quantity of the hydrated material, i.e., the stored energy, was measured. The release of energy upon hydration of the dried material, i.e., the reverse process, was monitored with a thermal camera. Although the measurements did not provide an exact quantity of the released energy per unit volume, the analysis showed that when putting a drop of water onto a layer of the dehydrated AlPO<sub>4</sub>-LTA powder, a sudden release of heat results in an increase of the sample temperature by about 50 °C, which is a remarkable value for materials (see Figure S5, Supporting Information). All the presented tests

suggest that AlPO<sub>4</sub>-LTA is really a highly promising energy-storage material, probably the best among the porous materials tested so far.

To take this argument further, effectiveness of AlPO<sub>4</sub>-LTA when used in a typical sorption heat-pump cycle was examined by calculating the thermodynamic efficiency (also called the coefficient of performance, COP) under several operating conditions. In order to facilitate comparison with MOFs, the procedure of de Lange et al. for the calculation of the per-cycle heat transfer for refrigeration and long-term storage was followed as closely as possible, as they examined not only MOF-801, but also many other materials, including two commercially available aluminophosphates.<sup>[7]</sup> Figure 5 and Figure S6 (Supporting Information) may be directly compared with their data (but note that MOF-801 has been recalculated, see the Supporting Information). We considered three use cases, heat pump, heat storage, and refrigeration, which are defined by the temperatures of evaporation and condensation. The definitions of the use cases, COP, stored heat, and heat transfer are given in the Supporting Information.

The COPs for AlPO<sub>4</sub>-LTA are compared to those of MOF-801, MIL-160, and AlPO<sub>4</sub>-34 (Figure S6, Supporting Information). All materials achieve comparable COPs at high desorption temperatures, but AlPO<sub>4</sub>-LTA requires desorption temperature 10–15 °C lower than other materials to achieve maximum efficiency. In our opinion, however, COP, if not too low, is not a very good metric for evaluating these materials. Thermodynamic efficiency translates to fuel efficiency, but the use cases assume that desorption is powered by solar heat and, thus, efficiency is less relevant. Instead, we focus on the effectiveness of the material when used in a heat pump, a refrigerator in particular. We are interested in the cooling power, i.e., the rate of heat removal through the evaporator, which depends on the cycling rate and the amount of heat removed in each cycle. The latter is shown in Figure 5a. Evidently, all materials considered here maintain useful levels of performance throughout the rather demanding range of temperature lifts, which is not the case with some otherwise promising MOFs, e.g., MOF-841.<sup>[7]</sup> We can see that COP gives a wrong impression for MOF-801, which, despite having a COP some 10% lower than MIL-160, outperforms it by between 17% and 35% when it comes to cooling power. The difference is even more pronounced for MIL-160 and AlPO<sub>4</sub>-LTA, which achieve comparable COPs, but the latter yields around 50% higher cooling power for a given volume and cycling rate.

**Table 1.** Crystal densities of dry materials, water uptakes, and energy-storage capacities per unit mass and unit volume for AlPO<sub>4</sub>-LTA, AlPO<sub>4</sub>-34, MOF-801, and MIL-160.

Sample	Crystal density <sup>a)</sup> [g cm <sup>-3</sup> ]	Water uptake <sup>a)</sup> (0.05–0.30) <sup>b)</sup>		Water uptake (0–0.9)		Energy capacity	
		[g g <sup>-1</sup> ]	[g cm <sup>-3</sup> ]	[g g <sup>-1</sup> ]	[g cm <sup>-3</sup> ]	[Wh kg <sup>-1</sup> ]	[kW h m <sup>-3</sup> ]
AlPO <sub>4</sub> -LTA	1.412	0.37	0.52	0.42	0.59	373	527
AlPO <sub>4</sub> -34	1.474	0.29	0.42	0.35	0.49	320	472
MOF-801	1.592	0.24	0.39	0.36	0.57	323	514
MIL-160	1.068	0.30	0.32	0.38	0.41		N. A.

<sup>a)</sup>Crystal density and water uptake for MIL-160 were obtained from the work of Cadiou et al.<sup>[9]</sup>; <sup>b)</sup>Values in parenthesis indicate the corresponding relative-pressure range.

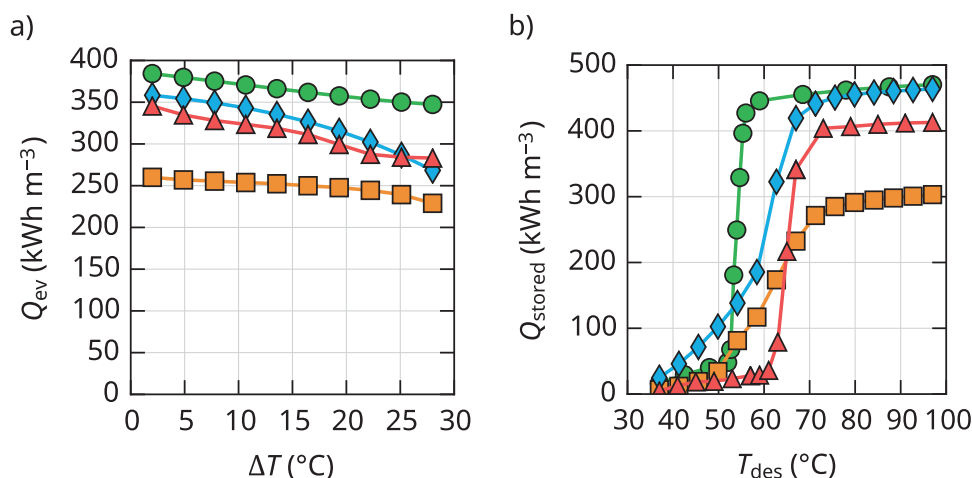


**Figure 5.** a) Heat transferred from the evaporator in one refrigeration cycle, per unit of adsorbent volume, as a function of temperature lift. b) Storable heat per unit of adsorbent volume as a function of desorption temperature. ALPO<sub>4</sub>-LTA (green ●), MIL-160 (orange ■), MOF-801 (blue ◆), and ALPO<sub>4</sub>-34 (red ▲).  $T_{con}$ ,  $T_{ev}$ , and  $T_{des}$  are temperatures of condenser, evaporator, and desorption temperature, respectively.  $\Delta T = T_{con} - T_{ev}$  at  $T_{con} = 30$  °C and  $T_{des} = 100$  °C. ALPO<sub>4</sub>-LTA exhibits the largest cooling power for refrigeration and attains the highest heat-storage capacity at the lowest temperature among the materials compared here.

For long-term heat storage, only the heat released during adsorption is considered, assuming that all sensible heat involved in the heat cycle (the “heat storage” use case defined in the Supporting Information) is dissipated and that the heat required to dry the adsorbent is abundant, as is the case with, e.g., seasonal heat storage. In Figure 5b we see that the storage capacity of ALPO<sub>4</sub>-LTA is on par with that of MOF-801, but the desorption temperature required to charge the material is lower for ALPO<sub>4</sub>-LTA by 10–15 °C. ALPO<sub>4</sub>-LTA attains 90% capacity at only 60 °C, making it more suitable for long-term solar-heat storage even in regions without extended periods of intense solar irradiation.

### 2.3. Understanding Hydration of ALPO<sub>4</sub>-LTA

To employ ALPO<sub>4</sub>-LTA as an energy-storage material in an adsorption-driven heat exchanger, or to find or design an even better energy-storage material, it is not enough only to determine the structural and sorption characteristics of this material but one needs also to understand its performance on the microscopic scale. A microscopic insight into the hydration of ALPO<sub>4</sub>-LTA can be obtained by the combined use of XRD and NMR spectroscopy. XRD patterns of the sample that was hydrated for varying periods of time are presented in Figure 2. They show broadened peaks that resemble a partly disordered structure. The broadening indicates that water molecules within the pores of the hydrated material do not exhibit long-range order, and that the varying arrangement of water molecules from one pore to another also induces small variations in the geometry of the aluminophosphate framework of ALPO<sub>4</sub>-LTA.

It is interesting that each diffraction pattern in the series can be very well described as a simple sum of two patterns, one belonging to completely dehydrated material and one to fully hydrated material. The decomposition of the diffraction patterns into these two contributions then allows one to see how the fraction of the hydrated phase increases with time. Figure S8

(Supporting Information) shows that after the initial jump, this fraction increases linearly with the time of hydration. Similar picture emerges from the analysis of <sup>1</sup>H MAS NMR spectra of the progressively hydrated ALPO<sub>4</sub>-LTA. Due to hydration, a peak at 5.4 ppm starts rising in the <sup>1</sup>H NMR spectra (Figure 6a). The peak belongs to water molecules adsorbed within the pores of ALPO<sub>4</sub>-LTA. Quantitative analysis of <sup>1</sup>H MAS NMR spectra shows that the amount of water within the pores increases linearly with the time of hydration (Figure 6b).

An additional insight into the hydration of ALPO<sub>4</sub>-LTA is offered by <sup>27</sup>Al MAS NMR spectroscopy. The dried calcined material exhibits a single relatively narrow aluminum signal with well-defined quadrupolar line-shape, which can be ascribed to four-coordinated aluminum atoms. Upon hydration, two additional broad contributions appear in the spectrum, one belonging to a new four-coordinated aluminum environment and the other belonging to six-coordinated aluminum atoms (Figure 6a). The change in aluminum coordination environment is very common for hydrated aluminophosphates and was, for example, thoroughly investigated in ALPO<sub>4</sub>-34. As the diffraction patterns, each <sup>27</sup>Al MAS NMR spectrum in the series can also be described as a simple sum of the spectrum of the completely dehydrated material and the spectrum of the completely hydrated material. The rate with which the fraction of the hydrated phase increases with time matches exactly the rate with which the amount of water in the sample increases (as determined from the <sup>1</sup>H MAS NMR spectroscopy). Throughout hydration, the ratio of the integrals of the two broad Al peaks, i.e., the ratio of the four-coordinated versus six-coordinated aluminum in the hydrated phase, is constantly equal to ≈1:2 (Figure 6b). This is very important and clearly shows that hydration of ALPO<sub>4</sub>-LTA follows a simple one-step mechanism: a single unit cell of ALPO<sub>4</sub>-LTA is instantly filled with the entire amount of water and is not filled layer by layer. In other words, we cannot detect the coordination of water to the framework aluminum and the adsorption of additional water molecules into the interior of the pore as two distinct steps. The observed

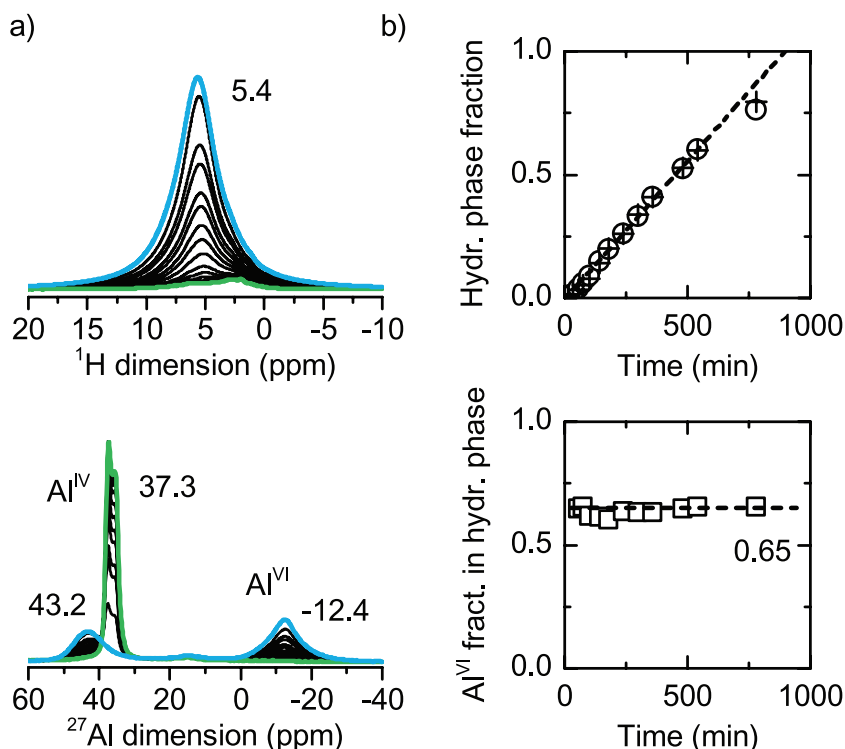


**Figure 6.** a)  $^1\text{H}$  and  $^{27}\text{Al}$  MAS NMR spectra of the completely dried (green), partially hydrated (black), and fully hydrated (blue)  $\text{AlPO}_4\text{-LTA}$ . b) Fraction of the hydrated phase versus the time during which the sample was exposed to the humid atmosphere (98% relative humidity). The fraction was determined by fitting the  $^1\text{H}$  MAS ( $\odot$ ) and  $^{27}\text{Al}$  MAS ( $\oplus$ ) spectra with a simple sum of the spectrum of the completely dehydrated material and the spectrum of the completely hydrated material. The contribution of the six-coordinated aluminum in the hydrated phase ( $\square$ ) remains nearly constant during hydration.

progressive hydration of the material is thus associated with the diffusion of water from pore to pore (which might be regarded almost as a jump of the entire water cluster from one pore to another) and from crystallite to crystallite through the sample along the axis of the NMR rotor (see **Figure 7**).

The described one-step hydration mechanism of  $\text{AlPO}_4\text{-LTA}$  is different from the mechanism encountered in many MOFs, including MOF-801 and MIL-160. Such MOFs possess bridging OH groups in the frameworks, which act as rather strong adsorption centers for water molecules. Calculations and XRD and NMR measurements show that during hydration water molecules first attach to these centers, and only in the second step additional water molecules enter the pores and form the hydrogen-bonded network in the interior.<sup>[9]</sup> Adsorption in such

MOFs is thus at least a two-step process, which leads to the less steep sorption isotherm of MOFs compared to the isotherm of  $\text{AlPO}_4\text{-LTA}$ .

The reason for the difference in the hydration mechanism can be better understood with the help of quantum chemical calculations. The calculations within the density functional theory (DFT) have been performed primarily on  $\text{AlPO}_4\text{-34}$  and MIL-160 since their intermediate structures have been very well resolved both experimentally and in previous DFT studies. While  $\text{AlPO}_4\text{-34}$  exhibits three phases of hydration,<sup>[14]</sup> we focus on the first phase whose mechanism matches that of  $\text{AlPO}_4\text{-LTA}$  and gives rise to the steep part of the adsorption isotherm. In this first phase of hydration, two out of six aluminum atoms of the crystallographic unit cell of  $\text{AlPO}_4\text{-34}$  get six-coordinated because of four water molecules that attach to them, and additional six water molecules adsorb into each chabazite cage and form a strongly hydrogen-bonded cluster in it. The aluminophosphate framework deforms significantly upon hydration. Starting with the hydrated structure and removing all water molecules except for the four that are bound to the aluminum atoms, geometry optimization yields practically no change to the framework, demonstrating that it is the difference in bond angles of the six-coordinated (around  $90^\circ$ ) versus the four-coordinated ( $110^\circ$ ) aluminum atoms that

affects the deformation of the framework and not the presence of the clusters of water molecules inside the chabazite cages. This is additionally confirmed by removal of all water and further geometry optimization, upon which the framework springs back toward the nondeformed high-symmetry state. It is interesting to leave only one water molecule attached, making one aluminum atom five-coordinated. Geometry optimization yields a change in framework deformation and, importantly, a very different binding energy. Binding energies, per molecule, are  $67\text{ kJ mol}^{-1}$  with ten water molecules in the chabazite pore (i.e., right after the steep jump in the isotherm),  $49\text{ kJ mol}^{-1}$  with four molecules (two six-coordinated aluminum atoms per one pore), and merely  $14\text{ kJ mol}^{-1}$  with one water molecule (one five-coordinated aluminum atom per one chabazite

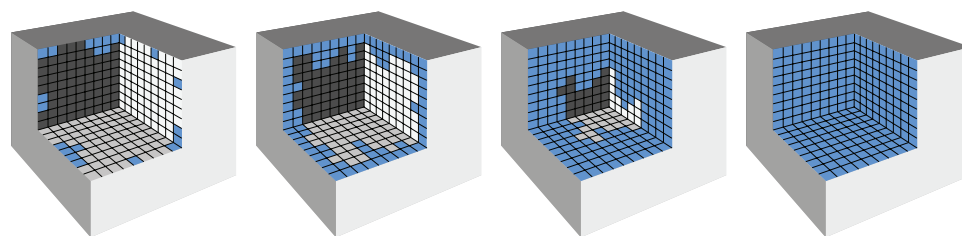


**Figure 7.** Schematic representation of the proposed pore-by-pore hydration mechanism of an  $\text{AlPO}_4\text{-LTA}$  crystallite. Hydration progresses from barely (left) to fully (right) hydrated in discrete steps; a single pore of  $\text{AlPO}_4\text{-LTA}$  is instantly and completely filled with water and there are no partially filled pores.

pore). This tells us that the chemical potential of water vapor must first increase enough to make certain aluminum sites six-coordinated. At that point, the structure becomes significantly more hydrophilic, as reflected by the much higher binding energy of additional water molecules. As the chemical potential is already high enough, the pore is readily filled with water. In other words, one can say that as soon as aluminum atoms of a given chabazite cage change coordination from fourfold to sixfold, water molecules instantly fill this particular cage, and they rather do that than attach to aluminum atoms of another cage.

Since the above described hydration mechanism is caused by framework changes induced by six-coordinated aluminum atoms, it is reasonably evident that the same mechanism is at work in  $\text{AlPO}_4\text{-LTA}$ . Although its unit cell does not change as much as that of  $\text{AlPO}_4\text{-34}$ , the framework must nonetheless be deformed. Unlike for  $\text{AlPO}_4\text{-34}$ , there is no quantitative experimental data on the deformation of  $\text{AlPO}_4\text{-LTA}$ , but a significant amount of framework disorder is evident from the broadening of the diffraction peaks. This indicates that deformation is present, although it does not exhibit long-range order. Preliminary DFT geometry optimization of water-filled  $\text{AlPO}_4\text{-LTA}$  supports this. Firmer evidence would be provided by more costly finite-temperature ab-initio molecular dynamics, which, given the size of  $\text{AlPO}_4\text{-LTA}$  unit cell, would be quite demanding and would merit a separate study.

Mechanism of hydration of many MOFs is different. In MIL-160, the first water molecules bind by two hydrogen bonds to framework hydroxyl groups and nearby Al–O–C bridging oxygens with a binding energy of  $55 \text{ kJ mol}^{-1}$ . During this step the framework does not change. The binding energy of additional water molecules is lower, so no more molecules are adsorbed and pores are not filled unless chemical potential is increased. The same mechanism of gradual pore filling, which nicely explains why MOFs have less steep adsorption isotherms than aluminophosphates, is expected also for MOF-801.

### 3. Conclusion

The small-pore aluminophosphate  $\text{AlPO}_4\text{-LTA}$  is an excellent material for sorption-based solar-energy allocation and storage, superior to all other zeolite-like and MOF materials tested so far. Its synthesis and calcination are quick and simple. The material adsorbs water in an extremely narrow pressure range and exhibits unprecedented water uptake and energy-storage capacity. It also shows remarkable cycling stability. In  $\text{AlPO}_4\text{-LTA}$ , energy is predominantly stored in the hydrogen-bonded clusters of water molecules within the pores. Interaction of water molecules with the aluminophosphate framework is weaker. Even though a large fraction of framework aluminum changes coordination from fourfold to sixfold upon hydration, framework aluminum atoms do not represent strong adsorption centers. Hydration of aluminum atoms deforms the aluminophosphate framework and triggers sudden pore filling and formation of water clusters. This mechanism gives rise to the extremely steep sorption isotherm of  $\text{AlPO}_4\text{-LTA}$ . The lack of strong adsorption centers facilitates dehydration of the aluminophosphate at low temperature. This important property

implies that regeneration (or charging) of the material in a solar-energy-storage system should be easily achieved using most common types of solar collectors, e.g., flat plate collectors, even in regions without extended periods of intense solar irradiation.  $\text{AlPO}_4\text{-LTA}$  exhibits also very high cooling power at large temperature lifts. The water-sorption mechanism within  $\text{AlPO}_4\text{-LTA}$  is very similar to the mechanism within another well-studied porous aluminophosphate,  $\text{AlPO}_4\text{-34}$ .  $\text{AlPO}_4\text{-LTA}$  outperforms  $\text{AlPO}_4\text{-34}$  as an energy-storage material mainly because of its larger pore volume. This suggests that perhaps an even more capable material than  $\text{AlPO}_4\text{-LTA}$  can be found among the microporous aluminophosphates with even larger pores.

### 4. Experimental Section

**Hydrothermal Synthesis:**  $\text{AlPO}_4\text{-LTA}$  material was hydrothermally synthesized from a reaction mixture with the following molar ratio of reactants  $\text{P}_2\text{O}_5$ :  $\text{Al}_2\text{O}_3$ : 0.5 K222: HF: 200  $\text{H}_2\text{O}$ . The chemicals, phosphoric acid ( $\text{H}_3\text{PO}_4$ , 85%, Merck), aluminum isopropoxide (AIP, 98%,  $\text{Al}_2\text{O}_3$ , Merck), hydrofluoric acid (HF, 48% in water, Merck), 4,7,13,16,21,24-Hexaoxa-1,10-diazabicyclo[8.8.8]hexacosane (K222, 98%, Acros), and distilled water, were all used as received. For a typical synthesis, 5.00 g AIP was added to 2.77 g  $\text{H}_3\text{PO}_4$  and 42.52 g distilled water. The mixture was stirred 30 min with Ultra Turax at room temperature before adding 2.26 g K222 and 0.5 g HF. The final mixture was again stirred for 20 min and then introduced into a Teflon-lined stainless steel autoclave. After crystallization at  $190^\circ\text{C}$  for 4 h,  $\text{AlPO}_4\text{-LTA}$  powder was filtered, washed with distilled water, and dried at  $105^\circ\text{C}$ . The as-synthesized product was calcined at  $850^\circ\text{C}$  for 2 h in air.

$\text{AlPO}_4\text{-34}$  was prepared according to the published procedure,<sup>[14]</sup> whereas synthesis of MOF-801 was performed by the modified procedure from Furukawa et al.,<sup>[8]</sup> with the same molar ratios of reaction components and synthesis conditions as described in the literature, but using  $\text{ZrCl}_4$  (99%, Sigma-Aldrich) instead of  $\text{ZrOCl}_2$ .

**X-ray Diffraction:** Structural changes during calcination, hydration, and dehydration were monitored by temperature-programmed X-ray diffraction on PANalytical X'Pert PRO high-resolution diffractometer in the  $2\theta$  range from  $5^\circ$  to  $50^\circ$  using a step of  $0.026^\circ$  per 100 s. During calcination, diffraction patterns were recorded in a flow of air in steps of  $100^\circ\text{C}$  from room temperature to  $900^\circ\text{C}$ . After letting the sample to cool down to room temperature, the temperature-programmed protocol was repeated twice in order to determine the structure stability and reversibility upon hydration/dehydration.

**NMR Spectroscopy:** Solid-state MAS NMR spectra were recorded on a 600 MHz Varian NMR system equipped with a 1.6 mm Varian MAS probe. Larmor frequencies for  $^1\text{H}$ ,  $^{27}\text{Al}$ , and  $^{31}\text{P}$  were 599.54 MHz, 156.22 MHz, and 242.69 MHz, respectively, and sample spinning frequency was 20 kHz.  $^1\text{H}$  spectra were recorded using a  $\pi/2$  excitation pulse with duration of 1.35  $\mu\text{s}$  and 32 scans. The delay between the scans was 5 s.  $^{27}\text{Al}$  spectra were collected with a  $\pi/4$  pulse of 0.5  $\mu\text{s}$ , 256 repetitions, and recycle delay of 1 s.  $^{31}\text{P}$  spectra were taken with a single scan, using a  $\pi/2$  excitation pulse of 1.1  $\mu\text{s}$ . Frequency axes of  $^1\text{H}$ ,  $^{27}\text{Al}$ , and  $^{31}\text{P}$  spectra were referenced to TMS, 0.1 M  $\text{Al}(\text{NO}_3)_3$  aqueous solution, and 85 wt%  $\text{H}_3\text{PO}_4$  solution in water. Prior to the NMR measurements, sample was packed in a rotor and dried at  $150^\circ\text{C}$  under vacuum for 2 h. Partial rehydration was performed by opening the rotor and placing it in the excicator with a controlled 98% relative humidity for a certain amount of time.

**Thermal and Sorption Analysis:** Thermogravimetric analysis was performed on a Q5000 IR thermogravimetric (TA Instruments, Inc.). The measurements were carried out in air flow ( $25 \text{ mL min}^{-1}$ ) with a heating rate of  $10^\circ\text{C min}^{-1}$ . Prior to measurements, the samples were exposed to controlled relative humidity of 75% for three days to ensure saturation with water vapor. Dynamic calorimetric measurements were performed

on a Q2000 DSC apparatus (TA Instruments, Inc.) in the temperature range from 25 to 200 °C with the heating ramp of 1 °C min<sup>-1</sup>.

Water sorption analysis was performed by an IGA-100 gravimetric analyzer (Hiden Isochema Ltd.). Water sorption isotherms were performed at different temperatures from 25 to 40 °C in the relative-pressure range from 0 to 0.9 in order to elucidate sorption enthalpies. Prior to measurements, the samples were degassed at 150 °C to a constant weight overnight. Hydration/dehydration cycling performance was carried out with the sequential procedure of isothermal measurements at 25 °C and relative humidity of 0.3 until equilibrium, followed by drying at 150 °C for 2 h in vacuum. The sequence was repeated 40 times.

**Thermodynamic Calculations:** The definition of the thermodynamic heat cycle and the calculation of the amount of heat involved are given by De Lange et al.<sup>[7]</sup> Best efforts were put in to match their procedure in order to provide data that can be easily compared. A short summary and the distinctive details about this approach are given in the Supporting Information, and the reader is referred to the excellent exposition of de Lange et al. for the rest.

**First-Principles Calculations:** Calculations were performed using Quantum ESPRESSO<sup>[22]</sup> (version 5.1.2), which is a pseudopotential-based plane-wave density functional theory software package. The functional employed was PBEsol,<sup>[23]</sup> which was shown to yield reasonable NMR chemical shifts in hydrated AlPO<sub>4</sub>-34,<sup>[14]</sup> accurately reproducing the experimental structure. Pseudopotentials were from PSLibrary,<sup>[24,25]</sup> version 1.0.0. The library provides two types of pseudopotentials for certain elements with different speed/accuracy tradeoffs; the more accurate versions were used, requiring 90 and 360 Ry plane-wave energy cutoffs for wavefunctions and densities, respectively, to achieve good force and stress convergence. While gamma-point calculations sufficed for AlPO<sub>4</sub>-LTA, a 2 × 2 × 2 Monkhorst-Pack<sup>[26]</sup> grid was employed for MIL-160 and AlPO<sub>4</sub>-34. In our previous work on the latter, we used a denser grid, which was not necessary in the present case since no NMR chemical shifts were calculated.

## Supporting Information

Supporting Information is available from the Wiley Online Library or from the author.

## Acknowledgements

This work was supported by the Slovenian Research Agency (Grant Nos. P1-0021, L1-7665, and J1-5447). Edi Kranjc is acknowledged for his help with XRD measurements.

Received: August 18, 2016  
Published online:

- [1] J. Jänchen, D. Ackermann, H. Stach, W. Brösicke, *Sol. Energy* **2004**, 76, 339.
- [2] S. K. Henninger, F. P. Schmidt, H.-M. Henning, *Appl. Therm. Eng.* **2010**, 30, 1692.
- [3] C. Janiak, S. K. Henninger, *Chimia* **2013**, 67, 419.
- [4] P. Tatsidjoudoug, N. Le Pierrès, L. Luo, *Renewable Sustainable Energy Rev.* **2013**, 18, 327.
- [5] N. Yu, R. Z. Wang, L. W. Wang, *Prog. Energy Combust. Sci.* **2013**, 39, 489.
- [6] Y. I. Aristov, *Appl. Therm. Eng.* **2013**, 50, 1610.
- [7] M. F. de Lange, K. J. F. M. Verouden, T. J. H. Vlugt, J. Gascon, F. Kapteijn, *Chem. Rev.* **2015**, 115, 12205.
- [8] H. Furukawa, F. Gándara, Y.-B. Zhang, J. Jiang, W. L. Queen, M. R. Hudson, O. M. Yaghi, *J. Am. Chem. Soc.* **2014**, 136, 4369.
- [9] A. Cadiou, J. S. Lee, D. Damasceno Borges, P. Fabry, T. Devic, M. T. Wharmby, C. Martineau, D. Foucher, F. Taulelle, C.-H. Jun, Y. K. Hwang, N. Stock, M. F. De Lange, F. Kapteijn, J. Gascon, G. Maurin, J.-S. Chang, C. Serre, *Adv. Mater.* **2015**, 27, 4775.
- [10] J. Jänchen, D. Ackermann, E. Weiler, H. Stach, W. Brösicke, *Thermochem. Acta* **2005**, 434, 37.
- [11] E. P. Ng, S. Mintova, *Microporous Mesoporous Mater.* **2008**, 114, 1.
- [12] A. Ristić, N. Z. Logar, S. K. Henninger, V. Kaučič, *Adv. Funct. Mater.* **2012**, 22, 1952.
- [13] M. Fischer, *Phys. Chem. Chem. Phys.* **2016**, 18, 15738.
- [14] J. Varlec, A. Krajnc, M. Mazaj, A. Ristić, K. Vanatala, A. Oss, A. Samoson, V. Kaučič, G. Mali, *New J. Chem.* **2016**, 40, 4178.
- [15] C. Baerlocher, L. B. McCusker, Database of Zeolite Structures, <http://www.iza-structure.org/databases>, accessed: August, 2016.
- [16] M. D. Foster, I. Rivin, M. M. J. Treacy, O. D. Friedrichs, *Microporous Mesoporous Mater.* **2006**, 90, 32.
- [17] L. Schreyeck, J. Stumbe, P. Caullet, J.-C. Mougénel, B. Marler, *Microporous Mesoporous Mater.* **1998**, 22, 87.
- [18] J. E. Schmidt, S. I. Zones, D. Xie, M. E. Davis, *Microporous Mesoporous Mater.* **2014**, 200, 132.
- [19] X. Zhao, J. Zhao, C.-Y. Chiang, Z. Li, Y. Zhao, W. Zhou, *New J. Chem.* **2016**, 40, 2444.
- [20] A. Huang, F. Liang, F. Steinbach, T. M. Gesing, J. Caro, *J. Am. Chem. Soc.* **2010**, 132, 2140.
- [21] E. J. Fayad, N. Bats, C. E. A. Kirschhock, B. Rebours, A.-A. Quoineaud, J. A. Martens, *Angew. Chem., Int. Ed. Engl.* **2010**, 49, 4585.
- [22] P. Giannozzi, S. Baroni, N. Bonini, M. Calandra, R. Car, C. Cavazzoni, D. Ceresoli, G. L. Chiarotti, M. Cococcioni, I. Dabo, A. Dal Corso, S. de Gironcoli, S. Fabris, G. Fratesi, R. Gebauer, U. Gerstmann, C. Gougoussis, A. Kokalj, M. Lazzeri, L. Martin-Samos, N. Marzari, F. Mauri, R. Mazzarello, S. Paolini, A. Pasquarello, L. Paulatto, C. Sbraccia, S. Scandolo, G. Sclauzero, A. P. Seitsonen, A. Smogunov, P. Umari, R. M. Wentzcovitch, *J. Phys.: Condens. Matter* **2009**, 21, 395502.
- [23] J. P. Perdew, A. Ruzsinszky, G. I. Csonka, O. A. Vydrov, G. E. Scuseria, L. A. Constantin, X. Zhou, K. Burke, *Phys. Rev. Lett.* **2008**, 100, 136406.
- [24] A. Dal Corso, *Comput. Mater. Sci.* **2014**, 95, 337.
- [25] A. Dal Corso, QEFORGE PSLibrary, <http://www.qe-forge.org/gf/project/pslibrary>, accessed: August, 2016.
- [26] J. D. Pack, H. J. Monkhorst, *Phys. Rev. B* **1977**, 16, 1748.